Multiple-Scales Analysis of Photonic Crystal Waveguides

Joyce Poon, *Student Member, IEEE*, Emanuel Istrate, *Student Member, IEEE*, Mathieu Allard, *Student Member, IEEE*, and Edward H. Sargent, *Member, IEEE*

Abstract—The multiple-scales method is used to derive a scalar differential equation that describes the envelopes of photonic crystal waveguide modes. For a photonic crystal heterostructure waveguide and an air core photonic crystal waveguide, the mode frequencies calculated from the envelope approximation and full numerical simulations agree to 9% in the worst case when compared to the frequency difference of the band edges. The single-mode and cutoff width conditions for a photonic crystal waveguide are predicted and verified.

Index Terms—Approximation methods, electromagnetic scattering by periodic structures, optical propagation in nonhomogenous media, optical waveguide theory, periodic structures.

I. INTRODUCTION

PHOTONIC crystal waveguides have been a subject of extensive experimental and theoretical study in recent years [1]–[6]. Line defects in photonic crystals can act as waveguides, where the stopband in the direction perpendicular to the propagation direction can provide an additional mechanism for mode confinement. However, the numerical simulations of these structures through finite difference time domain or plane wave expansion methods are computationally intensive. To lessen the computational complexity and to give a physical feel for waveguiding mechanisms in photonic crystals, theoretical work such as that based on the tight-binding approximation [7], [8] and coupled-mode analysis [9] has become an active area of research. In the former theory, the waveguide modes are treated as expansions of a localized Wannier function basis, whereas in the latter, the waveguide modes are considered as a superposition of plane waves reflected by the photonic crystal cladding.

In this paper, we present a physically intuitive, semi-analytical method to study photonic crystal waveguides. Our approach is inspired by the envelope function theory commonly used in semiconductor heterostructure physics. Our aim is to connect the properties of a photonic crystal waveguide to the dispersion relations of the constituent photonic crystals, for while full numerical simulations of photonic crystal waveguides are computationally intensive, dispersion relations of bulk photonic crystals can be readily computed.

Conventional photonic crystal waveguides made of line defects in photonic crystals can be more broadly classified as a type of photonic crystal heterostructure. Photonic crystal het-
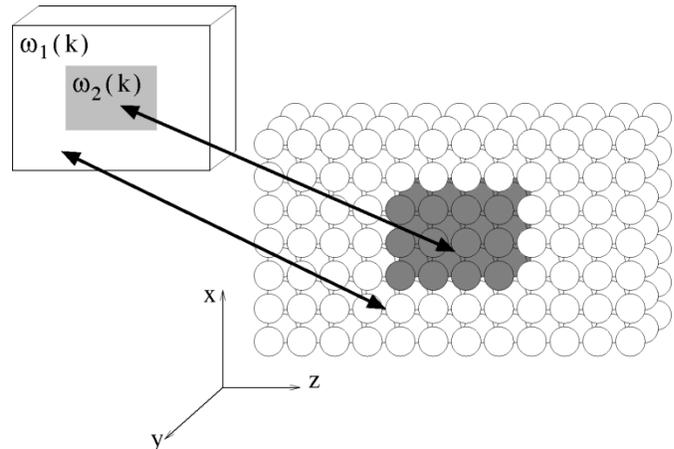
Fig. 1. Schematic of a photonic crystal heterostructure channel waveguide. The cladding and core regions are composed of photonic crystals characterized by dispersion relations $\omega_1(k)$ and $\omega_2(k)$, respectively.

erostructures are juxtapositions of materials with different dispersion relations (Fig. 1). In Fig. 1, waves can be guided along the heterostructure in the y direction.

We have previously derived envelope functions through Bloch mode expansions for photonic crystal heterostructure waveguides composed of photonic crystals with a small fractional index modulation [10]. In the present work, we show that the envelope picture may encompass a broader class of photonic crystal waveguides including those consisting of homogeneous (nonphotonic crystal) dielectric cores and those which guide in air.

In Section II, we use the multiple-scales method and the photonic crystal $k \cdot p$ theory described in the Appendix to derive a scalar envelope equation that describes the propagating modes in photonic crystal heterostructure waveguides. In Section III, we verify the envelope approximation for a slab heterostructure waveguide in a three-dimensional (3-D) photonic crystal by comparing its results with full numerical simulations. In Section IV, we apply the envelope approximation to a photonic crystal waveguide with an air core and validate our theoretical results with numerical simulations. We also derive and verify the single-mode and cutoff width conditions for the waveguide. In Section V, we discuss the implications and limitations of our theory.

II. THE ENVELOPE EQUATION

We use the multiple-scales method [11] to derive a general equation for a channel waveguide in a three-dimensional pho-

tonic crystal. The resultant envelope equation is analogous to the time-independent Schrodinger equation in an effective medium.

A. Multiple-Scales Derivation

In the multiple-scales method, we separate the photonic crystal heterostructure into two spatial length scales: 1) the fast-varying scale due to the lattice periodicity of the bulk photonic crystal and 2) the slowly varying scale due to the defect introduced by the waveguide core. We begin with the wave equation

$$\nabla^2 \mathbf{E} - \nabla(\nabla \cdot \mathbf{E}) = -\omega_n'^2 n^2(\mathbf{r})\mathbf{E} \tag{1}$$

where the speed of light c is normalized to 1, and the subscript n labels the eigenfrequencies of the waveguide modes ω'.

Our envelope approximation allows different photonic crystals in the core and cladding by solving the multiple-scales problem in the core and cladding separately. We adopt the coordinates shown in Fig. 1. We define μ as the perturbation parameter and set X and Z as the slow variables such that

$$X = \mu x, \quad Z = \mu z. \tag{2}$$

Furthermore, we assume that the corrections to the eigenfrequencies of the cladding and core, ω_{n1} and ω_{n2}, respectively, are

$$\omega_n'^2 = \omega_{ni}^2 + \mu\Omega_i^{(1)} + \mu^2\Omega_i^{(2)} + \mu^3\Omega_i^{(3)} + \cdots, \quad i = 1, 2. \tag{3}$$

Throughout the paper, the subscript i will associate a quantity to the bulk cladding ($i = 1$) or core ($i = 2$) materials.

The waveguide eigenmode is assumed to be

$$\mathbf{E}_i = \mathbf{e}_{0i} + \mu\mathbf{e}_{1i} + \mu^2\mathbf{e}_{2i} + \cdots \tag{4}$$

where $\mathbf{e}_i$ represents the different orders of the expansion.

We assume the multiple-scales equations can be solved in a piecewise manner in the core and cladding. Furthermore, we assume interband mixing is negligible so that the solution takes the form of a Bloch mode modulated by an envelope function. If the waveguide core is sufficiently wide compared to the period of the photonic crystals and can be considered as a weak index perturbation in the bulk cladding photonic crystal, we may assume that the envelope modulates the Bloch modes of the constituent photonic crystals near the center of and far away from the core. The zeroth-order term then takes the form

$$\mathbf{e}_{0i} = A(X, Z)\tilde{\phi}_{n\mathbf{k}i} \tag{5}$$

where $A(X, Z)$ is the envelope function and $\tilde{\phi}_{n\mathbf{k}i}$ is an electric-field eigenmode

$$\tilde{\phi}_{n\mathbf{k}i} = \exp(i\mathbf{k} \cdot \mathbf{r})|\mathbf{u}_{n\mathbf{k}i}\rangle \tag{6}$$

where the subscripts $\mathbf{k}$ and n label the wavevector and band number respectively. We have also adopted the Dirac notation, treating the electric-field Bloch mode $\mathbf{u}_{n\mathbf{k}i}(\mathbf{r})$ as a state function $|\mathbf{u}_{n\mathbf{k}i}\rangle$. Since the system is perturbed only in the x and z directions, the envelope should only be a function of these two directions. Analogous to the analysis by de Sterke and Sipe [12], our ansatz for the higher order terms is

$$\mathbf{e}_{1i} = \sum_{l \neq n} B_{l\mathbf{k}}(X, Z)\tilde{\phi}_{l\mathbf{k}i}$$

$$\mathbf{e}_{2i} = \sum_{m \neq n} C_{m\mathbf{k}}(X, Z)\tilde{\phi}_{m\mathbf{k}i} \tag{7}$$

where the rest of the higher order expansion terms are analogously defined. Each order is represented by a sum over the other electric-field Bloch modes at the wavevector corresponding to $\tilde{\phi}_{n\mathbf{k}i}$, with each Bloch mode modulated by an arbitrary envelope function, which for the $O(\mu)$ and $O(\mu^2)$ terms are $B_{l\mathbf{k}}(X, Z)$ and $C_{m\mathbf{k}}(X, Z)$, respectively.

We now proceed to substitute (4) into the wave equation and equate each order of the equation to zero. In the multiple-scales method, we treat the slow and fast variables independently. For example, when differentiating, we would write

$$\frac{\partial A}{\partial x} = \mu\frac{\partial A(X, Z)}{\partial X}. \tag{8}$$

Therefore, to $O(1)$, we simply have the unperturbed equation. Projecting the equation obtained in $O(\mu)$ to $1/V\langle\mathbf{u}_{n\mathbf{k}i}|$ and invoking relation (32) yields

$$\left(\frac{\partial A}{\partial Z}\right)\left(\frac{\partial\omega_{ni}^2}{\partial k_{zi}}\right) + \left(\frac{\partial A}{\partial X}\right)\left(\frac{\partial\omega_{ni}^2}{\partial k_{xi}}\right) + \Omega_i^{(1)}A = 0. \tag{9}$$

Since the slopes of the bands and the frequency corrections are real-valued and the envelope is not constant in both X and Z for a channel waveguide mode, for solutions that do not only exponentially decay or grow, we require

$$\Omega_i^{(1)} = 0 \tag{10}$$

$$\frac{\partial\omega_{ni}^2}{\partial k_{zi}} = \frac{\partial\omega_{ni}^2}{\partial k_{xi}} = 0. \tag{11}$$

Equation (11) stipulates that we must expand our solution about a band extremum in the directions perpendicular to the propagation direction.

Projecting the $O(\mu)$ equation to $1/V\langle\mathbf{u}_{l\mathbf{k}i}|$ and grouping the like terms result in an equation for $B_{l\mathbf{k}}$

$$B_{l\mathbf{k}} = \frac{1}{V}\frac{\frac{\partial A}{\partial X}\left\langle\mathbf{u}_{l\mathbf{k}i}\left|\widetilde{\mathbf{W}}_{xi}\right|\mathbf{u}_{n\mathbf{k}i}\right\rangle + \frac{\partial A}{\partial Z}\left\langle\mathbf{u}_{l\mathbf{k}i}\left|\widetilde{\mathbf{W}}_{zi}\right|\mathbf{u}_{n\mathbf{k}i}\right\rangle}{\omega_{li}^2 - \omega_{ni}^2} \tag{12}$$

where $\widetilde{\mathbf{W}}_{xi}$ and $\widetilde{\mathbf{W}}_{zi}$ are defined in (27)–(29).

We then proceed to gather all the $O(\mu^2)$ terms and project the equation to $1/V\langle\mathbf{u}_{n\mathbf{k}i}|$. When we substitute $B_{l\mathbf{k}}$ from (12) and simplify our relations for the band curvatures with (35), we finally arrive at our envelope equation

$$\frac{1}{2m_{xi}}\frac{\partial^2 A}{\partial X^2} + \frac{1}{2m_{zi}}\frac{\partial^2 A}{\partial Z^2} + \Omega_i^{(2)}A = 0 \tag{13}$$

where, in analogy to the effective mass in semiconductor physics, we have defined

$$\frac{1}{m_{xi}} = \frac{\partial^2\omega_{ni}^2}{\partial k_{xi}^2}, \quad \frac{1}{m_{zi}} = \frac{\partial^2\omega_{ni}^2}{\partial k_{zi}^2}. \tag{14}$$

By terminating the multiple-scales expansion in the second order, we have made a parabolic band approximation in the transverse directions of the waveguide. As our comparisons with numerical simulations will illustrate, a parabolic approximation is sufficiently accurate in describing the photonic crystal band structure.

Equation (13) is completely analogous to the envelope equation for semiconductor heterostructures. The only unknowns in the equation are $\Omega_1^{(2)}$, $\Omega_2^{(2)}$, and the envelope function A, for which we may solve by enforcing boundary conditions at the interfaces.

Applying (13) to the waves in an infinitely periodic photonic crystal results in the following relation between frequency and propagation vector perturbations:

$$\omega_n'^2 - \omega_n^2 = \frac{k_x'^2}{2m_x} + \frac{k_z'^2}{2m_z} \tag{15}$$

where k_x' and k_z' are the corrections to the propagation vectors. This is the well-known parabolic band expansion, which follows naturally from our analysis since we terminated it at the second order. The envelope equation provides an approximation to the dispersion relation of photonic crystal structures, including the infinitely periodic crystal.

B. Waveguiding Conditions

To illustrate the waveguiding mechanism, we consider a slab waveguide for which analytical solutions can be readily obtained. For a slab waveguide, the heterostructure profile is along z only. Thus, we drop the terms that depend on X in (13).

For a guide of width $2L$ along Z, the solutions of the envelope equation are

$$A(Z) = \begin{cases} B\cos(KZ) + C\sin(KZ), & |Z| < L \\ De^{-\gamma Z}, & Z > L \\ Fe^{\gamma Z}, & Z < -L \end{cases} \tag{16}$$

where γ and K are

$$\gamma = \sqrt{-2m_{z1}\Omega_1^{(2)}}, \quad K = \sqrt{2m_{z2}\Omega_2^{(2)}}. \tag{17}$$

We solve for the coefficients in (16) with appropriate boundary conditions. Although the boundary conditions at the interfaces between semiconductor crystals with dissimilar lattices remain a subject of contention [13]–[16], we shall assume that the envelope and its derivative are continuous across the boundaries. We solve the envelope equation by finding the appropriate $\Omega_1^{(2)}$ and $\Omega_2^{(2)}$ that match these boundary conditions. In general, heterostructure and dielectric boundaries do not coincide in space; hence, we do not apply the boundary conditions for fields in dielectric media.

From (16), we can determine the condition for waveguiding. The conditions on the curvatures of the envelope of a guided mode in the core and in the cladding necessitate that $\Omega_i^{(2)}$ and m_{zi} are of the same sign, implying that m_{z1} and m_{z2} must also be of the same sign. As illustrated in Fig. 2, these requirements on the band curvatures dictate that in the vicinity of the band extremum, the frequency allowed in the core is not allowed in the cladding. This condition on band curvatures, along with the condition on the slopes of the bands as given in (11), ensures
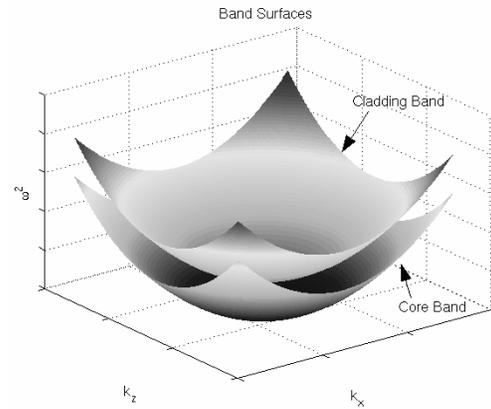

Fig. 2. Schematic of core and cladding bands for $\epsilon_{\text{core}} > \epsilon_{\text{clad}}$. The guided frequencies lie between the two bands.

that a guided wave propagates straight down the core with a frequency allowed in the core but not in the cladding.

III. PHOTONIC CRYSTAL HETEROSTRUCTURE WAVEGUIDES

To test the validity of the envelope approximation, we begin by comparing our theoretical results with those of full numerical simulations of a slab photonic crystal heterostructure waveguide in a three-dimensional photonic crystal. While the multiple-scales method is generally applicable to channel waveguides as illustrated in Fig. 1, due to the intensive nature of full 3-D numerical simulations and the complexity associated with the fabrication of such structures, we concentrate instead on slab waveguides. The envelope approximation is expected to hold best when the Bloch modes of the core are similar to those of the cladding; hence, we start by presenting results from a heterostructure whose core is a mildly perturbed version of the cladding material.

A. Numerical Results

We use MIT Photonic Bands (MPB) software [19] to simulate the heterostructure waveguides and to obtain the band curvatures. Fig. 3 illustrates the simulated structure. For simplicity, the photonic crystal considered is a cubic lattice of spheres with a radius of $0.5a$, where a is the lattice parameter. The simulation space is 20 cells wide in total, where the waveguide core is 5 cells wide and the cladding is 15 cells wide. The core consists of spheres with dielectric constant 10 in air ($\epsilon_{\text{core}} = 10$, 1), while the cladding consists of spheres with dielectric constant 11 in air ($\epsilon_{\text{clad}} = 11$, 1). Although MPB applies periodic boundary conditions, we find the cladding region is sufficiently wide to minimize coupling among adjacent waveguides. We examine the first band, and for a negative m_z, we use $k_z = \pi/a$. The propagation vector k_y is varied, while k_x is fixed at 0.

Due to the symmetry of the bulk photonic crystal, the first two bands are degenerate, corresponding to the quasi-transverse electric (TE) polarization, where the electric field is strongly polarized along x, and the quasi-transverse magnetic (TM) polarization, where the electric field is strongly polarized along y and z. We have not accounted for degeneracies in our multiple-scales derivation and shall assume that the degenerate Bloch modes share the same envelope. This approximation is valid
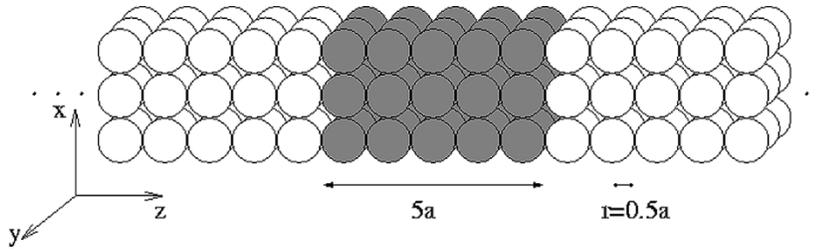
Fig. 3. Slab heterostructure waveguide simulated. The photonic crystal consists of a cubic lattice of spheres with $r = 0.5a$, where a is the lattice constant. The dielectric constants of the core and cladding are $\epsilon_{\mathrm{core}} = 10, 1$ and $\epsilon_{\mathrm{clad}} = 11, 1$ respectively. The waveguide core is 5 cells wide. The supercell is 20 cells wide. The structure is periodic along x and y.
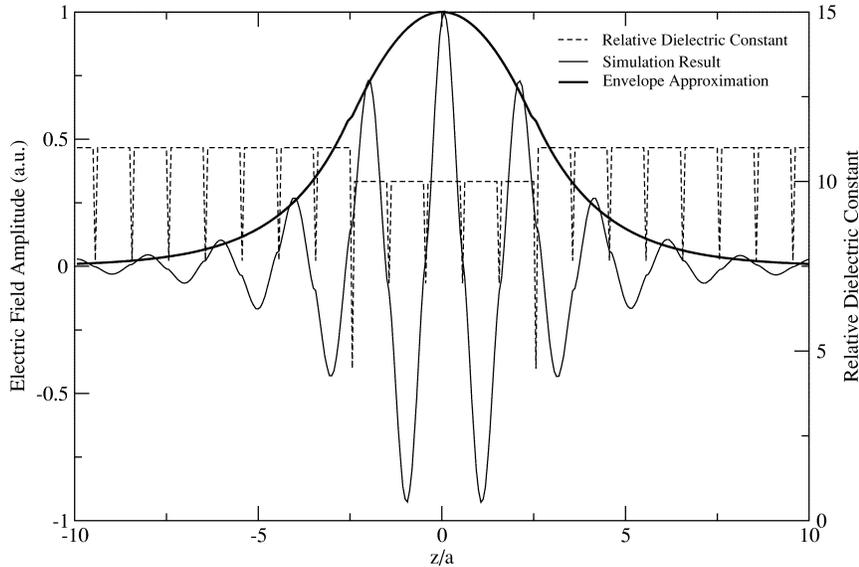

Fig. 4. Photonic crystal heterostructure waveguide mode at $k_{\mathrm{prop}} = \pi/a$. The x component of the electric field is shown. The simulation parameters are illustrated in Fig. 3.

for weak perturbations which do not cause significant coupling between the degenerate eigenstates, even if such coupling is present.

We compare the envelope to the main components of the electric field. The envelope approximation agrees well with the simulated results. Fig. 4 shows a representative mode shape, and Fig. 5 shows the dispersion relation. For this simulation, we generally do not observe quasi-TM modes which are present in the simulation of a heterostructure waveguide with a high index core. In the worst case, when compared to the frequency difference between the core and cladding bands, our predicted mode frequencies agree with the simulated result to 9%. Generally, the frequencies agree to about 5%.

IV. WAVEGUIDES WITH HOMOGENEOUS CORES

Since physical realizations of and experiments on photonic crystal heterostructure waveguides described in the previous section remain to be demonstrated, we apply the envelope approximation to conventional photonic crystal waveguides. To date, fabricated photonic crystal waveguides often consist of a homogeneous dielectric or air core surrounded by a photonic crystal cladding [3], [4], [17], [18]. Although the envelope approximation has not accounted for the finiteness

of the photonic crystal in the direction perpendicular to the plane of periodicity as in a photonic crystal slab, it can solve two-dimensional photonic crystal waveguides.

For a homogeneous material, our condition that $\partial\omega_{n2}^2/\partial k_{x2} = 0$ and $\partial\omega_{n2}^2/\partial k_{z2} = 0$ necessitates that we expand about $k_{x2} = 0$ and $k_{z2} = 0$. Moreover, the band curvature is constant and positive, with $\partial^2\omega_{n2}^2/\partial k_{x2}^2, \partial^2\omega_{n2}^2/\partial k_{z2}^2 = 2/n^2$. Therefore, in our envelope approximation, we can only solve for guided modes with reference to a photonic crystal band which is at a higher frequency than the core band.

The mode frequency is still expressed as a perturbation relative to the pertinent band extrema in the homogeneous core and the photonic crystal cladding. Thus, we may expect that the core dispersion relation should not deviate much from that of the cladding. Although the constraint may seem to limit the versatility of the envelope approximation, we shall see from numerical results that the envelope approximation is sufficiently robust that it can accurately solve a waveguide which represents a significant perturbation in the photonic crystal.

A. Numerical Results

We compare the predicted results from the envelope approximation with full numerical simulations. We use MPB to sim-
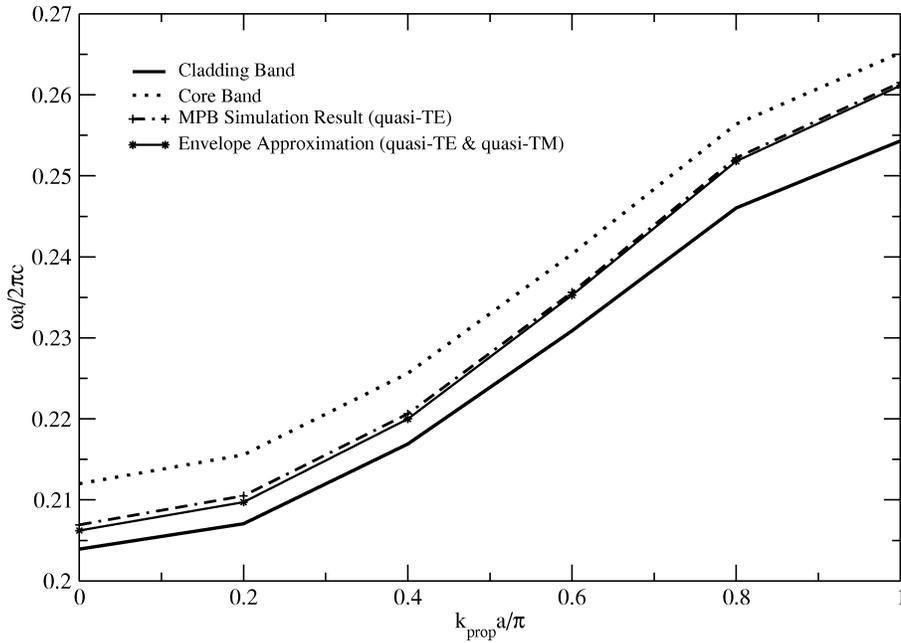
Fig. 5.   Dispersion relation of the photonic crystal heterostructure waveguide. The simulation parameters are illustrated in Fig. 3. The envelope equation gives the same dispersion relation for quasi-TE and quasi-TM modes.

Fig. 6.   Slab photonic crystal waveguide simulated. The photonic crystal consists of rods with $\epsilon = 12$ and $r = 0.2a$, where a is the lattice constant. Five missing rows of rods form the waveguide core. The supercell is 20 cells wide. The structure is periodic along y.

ulate the TE[1] modes of a slab waveguide with an air core in a two-dimensional (2-D) photonic crystal consisting of a square lattice of rods. Fig. 6 illustrates the simulated structure. The rods have a dielectric constant of 12 and a radius of $0.2a$. We examine the TE modes, since a transverse stopband exists for this polarization for the photonic crystal geometry and dielectric contrast. The structure simulated consists of a 5–cells-wide core and 15–cells-wide cladding.

For this waveguide, we find excellent agreement between the envelope approximation and simulated results. Fig. 7 shows some representative mode profiles, and Fig. 8 shows the dispersion relation. Solutions of the envelope equation whose frequencies are lower than the lower photonic crystal band edge are considered extraneous and ruled out. The higher propagation frequencies tend to show better agreement as the offset from the bulk photonic crystal band can be more appropriately described as a perturbed quantity. When compared to the frequency difference between the photonic crystal band edges, the propagation frequencies from the envelope approximation agree with simulated results to 9% in the worst case. On average, the frequencies agree to about 3%.

[1]In our coordinates, where the rods are parallel to x, TE waveguide modes are characterized by E_x, H_y, and H_z and are equivalent to the TM polarization in MPB.

B. Single-Mode and Cutoff Width Conditions

As a useful measure of the accuracy of the envelope approximation, we derive the single-mode and cutoff conditions for a slab air core waveguide and compare our predictions with the results from numerical simulations. For a slab waveguide of width $2L$, we solve (16) with the appropriate boundary conditions and find the waveguide is single mode for

$$\tan^{-1} \sqrt{\frac{m_1\left(\omega_1^2 - \omega^2\right)}{m_2\left(\omega^2 - \omega_2^2\right)}} \leq \sqrt{2m_2\left(\omega^2 - \omega_2^2\right)}L$$

$$< \frac{\pi}{2} + \tan^{-1}\sqrt{\frac{m_1(\omega_1^2 - \omega^2)}{m_2(\omega^2 - \omega_2^2)}}$$

$$(18)$$

where ω is the frequency of interest, and ω_1 and ω_2 are the unperturbed frequencies of the cladding and core bands respectively. All of these values are taken at $k_{\text{prop}} = 0$, which marks the onset of the waveguide modes.

Solving (18) for the photonic crystal described in this section and light of frequency $0.35c/a$, we find an air core waveguide remains single mode for $2L < 1.95a$. Numerical simulations using MPB show that the waveguide begins to support two modes when $2L$ is between $2a$ and $2.125a$. We also find that at this frequency, light cannot propagate when $2L \leq 0.52a$, while the numerical simulations show the cutoff waveguide width to be between $0.5a$ and $0.625a$. The envelope approximation gives excellent agreement with the results from numerical simulations, since there may also be inherent numerical errors due to the simulation software.

V. DISCUSSION

The envelope approximation is robust. It may be applicable to the study and design of a wide range of complex photonic
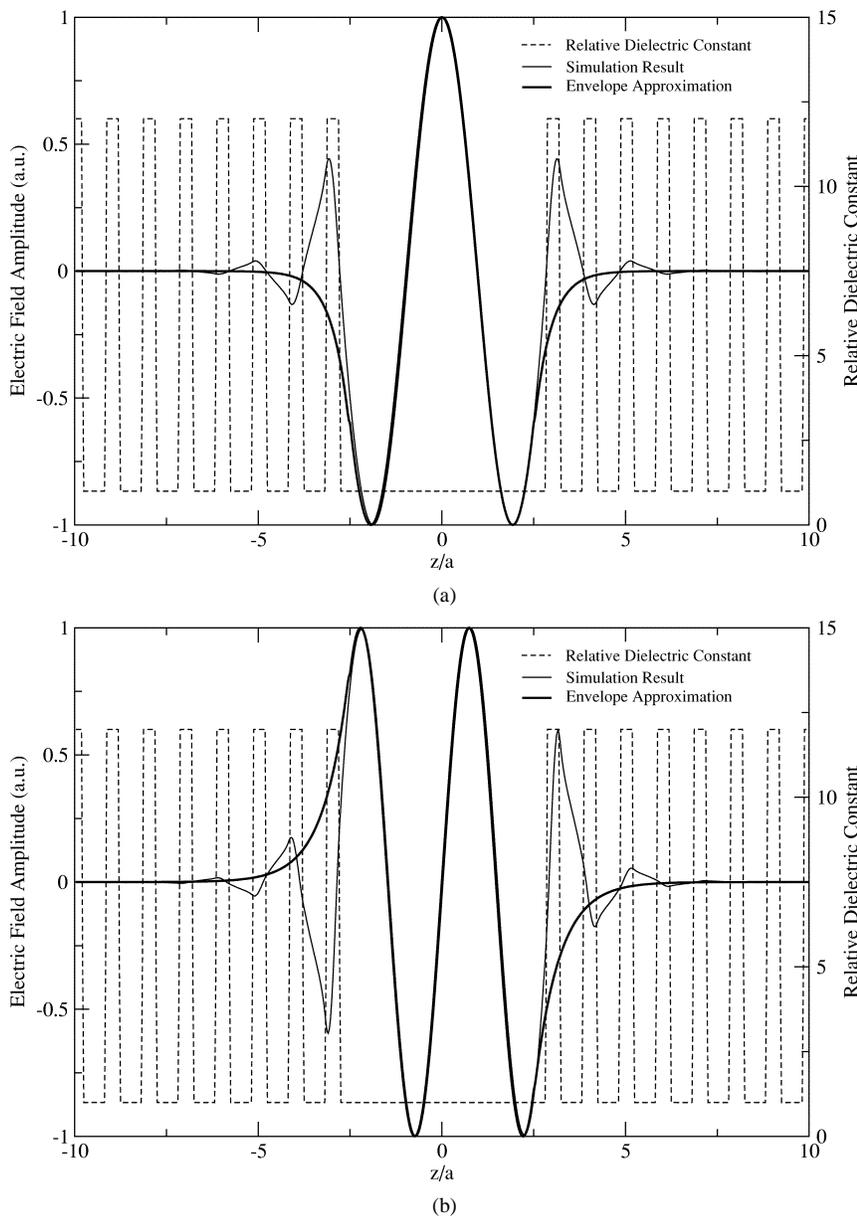
(a)

(b)

Fig. 7.   Two of the photonic crystal waveguide modes at $k_{\mathrm{prop}} = 0.4\,\pi/a$. (a) The mode corresponding to Even Mode 2 in Fig. 8. (b) The mode corresponding to Odd Mode 1. The x component of the electric field is shown. The simulation parameters are illustrated in Fig. 6.

crystal structures which may not satisfy the *a priori* envelope assumptions exactly. Moreover, while the actual electric and magnetic fields of the waveguide modes are vectorial and exhibit polarization dependence, the envelope approximation transcends these "microscopic" field properties by describing the modulating functions that encapsulate the general properties of the waveguide modes.

While only a single core band and a single cladding band are sufficient for the analyses of the waveguides presented here, more generally, multiple core and cladding bands may need to be considered, depending on the frequency range and size of photonic band gap as well as the geometry and the dispersion of the core. Moreover, since we consider a photonic crystal waveguide as in Fig. 6 rather than a photonic crystal holey fiber [20], there exists a periodicity in the propagation direction. Therefore, in a multiband treatment, the dispersion relations cannot be solved with reference to each core or cladding band independently, since the dispersion relations will be perturbed at frequencies where they cross, forming mini-stopbands [21]. A fully developed envelope theory will be a multiband approach that accounts for inter-band mixing, as well as complexities arising from the periodicity in the direction of propagation.

VI. CONCLUSION

Using the method of multiple scales, we have derived a scalar equation that describes photonic crystal waveguide modes. The band curvatures in the directions perpendicular to the waveguide, as abstracted from the dispersion relations of the constituent photonic crystals, act as homogenized dispersion relations which account for the local interactions of light with the photonic crystal. Comparisons between envelope solutions and full numerical simulations show the mode shapes and the dispersion relations are in excellent agreement. We illustrate a de-
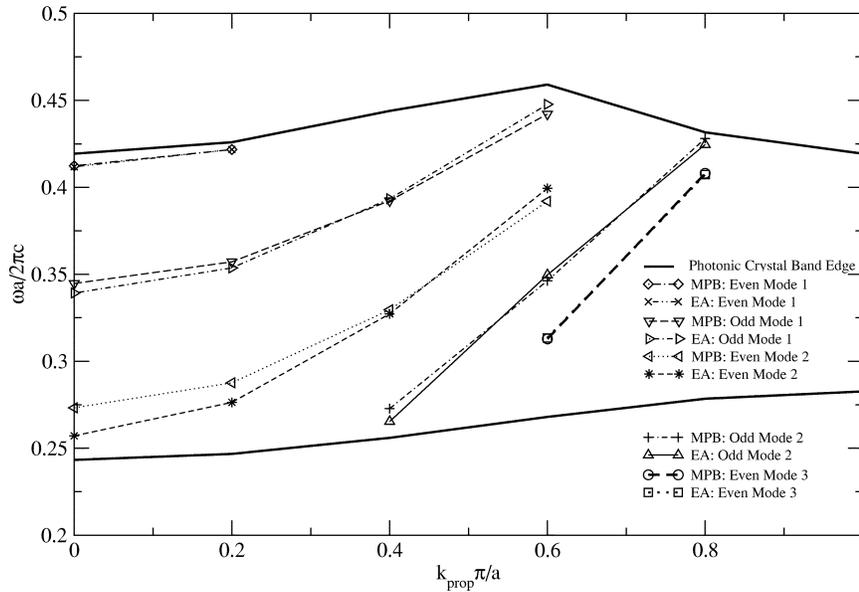
Fig. 8. Dispersion relation of the TE modes for the photonic crystal waveguide. The simulation parameters are illustrated in Fig. 6.

sign application of the envelope approximation by finding the guiding conditions, and the single-mode and cutoff widths for slab photonic crystal waveguides.

The envelope approximation is an efficient design tool for photonic crystal waveguides, reducing the computational complexities associated with full numerical simulations. The work presented here can also be used to study other devices such as directional couplers, resonators, and filters.

APPENDIX

Completing the multiple-scales expansion requires some results from a $k \cdot p$ theory for photonic crystals. Although more complete and rigourous research on photonic crystal $k \cdot p$ theory has been undertaken to study nonlinearity in photonic crystals [22], [23], such work cannot be directly applied to our envelope approximation. We shall derive an alternate formulation of the photonic crystal $k \cdot p$ theory that will not only serve our multiple-scales expansion but also show the regimes where our envelope approximation will be most applicable.

We begin with the vector wave equation

$$\nabla^2 \mathbf{E} - \nabla(\nabla \cdot \mathbf{E}) = -\omega_n^2 n^2(\mathbf{r})\mathbf{E} \tag{19}$$

where we have normalized $c = 1$, $n(\mathbf{r})$ is the refractive index of the photonic crystal, and the subscript n labels the eigenfrequencies of the photonic crystal, ω_n. In a periodic medium, the solutions to the wave equation are

$$\mathbf{E}_{n\mathbf{k}}(\mathbf{r}) = \mathbf{u}_{n\mathbf{k}}(\mathbf{r})\exp(i\mathbf{k} \cdot \mathbf{r}) \tag{20}$$

where the subscripts n and $\mathbf{k}$ label the band and wavevector corresponding to a Bloch mode of the electric field $\mathbf{u}_{n\mathbf{k}}(\mathbf{r})$. The electric-field Bloch modes will satisfy the orthonormality relation

$$\frac{1}{V}\left\langle \mathbf{u}_{m\mathbf{k}'}|n^2|\mathbf{u}_{n\mathbf{k}} \right\rangle = \delta_{m,n}\delta_{\mathbf{k}',\mathbf{k}} \tag{21}$$

where we have adopted the Dirac notation, and V is the volume of the cell which fixes the normalization of the Bloch modes. In the derivation that follows, we will use the Dirac notation, treating $\mathbf{u}_{n\mathbf{k}}(\mathbf{r})$ as a state function $|\mathbf{u}_{n\mathbf{k}}\rangle$.

Now we consider a perturbation in the wavevector to a particular electric-field mode, so the new electric field takes the form

$$\mathbf{E}'_{n\mathbf{k}'} = \exp\left(i\mathbf{k}' \cdot \mathbf{r}\right)|\mathbf{u}_{n\mathbf{k}'}\rangle \tag{22}$$

where

$$\mathbf{k}' = \mathbf{k_0} + \mu\tilde{\kappa}. \tag{23}$$

μ is the small perturbation parameter and $\tilde{\kappa}$ is the perturbation wavevector.

Following perturbation analysis, we assume the new Bloch mode will take the form

$$|\mathbf{u}_{n\mathbf{k}'}\rangle = |\mathbf{u}_{n\mathbf{k}}\rangle + \mu\left|\mathbf{u}_{n\mathbf{k}}^{(1)}\right\rangle + \mu^2\left|\mathbf{u}_{n\mathbf{k}}^{(2)}\right\rangle + \cdots \tag{24}$$

where the superscripts denote the orders of the Bloch mode correction. We also assume the eigenvalue correction is represented by

$$\omega_n'^2 = \omega_n^2 + \mu\lambda^{(1)} + \mu^2\lambda^{(2)} + \cdots \tag{25}$$

where $\lambda^{(n)}$ gives the nth-order correction to the eigenvalue.

We substitute our perturbed Bloch mode into the wave equation, and we find

$$\left(\mathbf{H_0} + \mu\mathbf{W} + \mu^2\mathbf{W}' + \ldots\right)|\mathbf{u}_{n\mathbf{k}'}\rangle = -\omega_n'^2 n^2 |\mathbf{u}_{n\mathbf{k}'}\rangle \tag{26}$$

where $\mathbf{H_0}$ acts as the unperturbed field operator analogous to a free Hamiltonian in quantum mechanics, while $\mathbf{W}$ and $\mathbf{W}'$ are the normalized perturbation operators. By expanding the wave equation in Cartesian coordinates, we can define three components $(\hat{x}, \hat{y}, \hat{z})$ to each vector operator. The action of each component of these operators on each component of a Bloch mode (u_x, u_y, u_z) follows explicitly.

If we define the three vector components of $\mathbf{W}$, $\mathbf{W_x}$, $\mathbf{W_y}$, and $\mathbf{W_z}$, we can alternatively define operators $\widetilde{\mathbf{W}}_x$, $\widetilde{\mathbf{W}}_y$, and $\widetilde{\mathbf{W}}_z$, such that

$$\widetilde{\mathbf{W}}_x = \kappa_x \frac{\partial}{\partial \kappa_x} (\mathbf{W_x} + \mathbf{W_y} + \mathbf{W_z}) \tag{27}$$

$$\widetilde{\mathbf{W}}_y = \kappa_y \frac{\partial}{\partial \kappa_y} (\mathbf{W_x} + \mathbf{W_y} + \mathbf{W_z}) \tag{28}$$

$$\widetilde{\mathbf{W}}_z = \kappa_z \frac{\partial}{\partial \kappa_z} (\mathbf{W_x} + \mathbf{W_y} + \mathbf{W_z}) \tag{29}$$

where we have just separated the perturbation dependences of the operators. A key property of $\mathbf{W}$ is that it is an adjoint operator. In other words, $\langle \mathbf{v_k}|\mathbf{W}|\mathbf{u_k}\rangle = \langle \mathbf{u_k}|\mathbf{W}|\mathbf{v_k}\rangle^*$. This property is a consequence of the periodic nature of Bloch modes.

Analogous to $k\cdot p$ theory in solid-state physics, we shall adopt the same approach as time-independent perturbation theory in quantum mechanics to solve our perturbed system. We shall obtain equations for each order of the perturbation expansion that will relate certain properties of the bandstructure to the Bloch modes.

The first-order correction to the eigenfrequency is a familiar result in quantum mechanics

$$\lambda^{(1)} = -\frac{1}{V} \langle \mathbf{u}_{n\mathbf{k}}|\mathbf{W}|\mathbf{u}_{n\mathbf{k}}\rangle. \tag{30}$$

A Taylor expansion about the eigenvalue corresponding to $|\mathbf{u}_{n\mathbf{k}}\rangle$ leads to an expression for $\lambda^{(1)}$

$$\lambda^{(1)} = \kappa_x \frac{\partial \omega_n^2}{\partial k_x} + \kappa_y \frac{\partial \omega_n^2}{\partial k_y} + \kappa_z \frac{\partial \omega_n^2}{\partial k_z}. \tag{31}$$

Therefore, simplifying (30) and separating the κ_x, κ_y, and κ_z dependences give our the set of relations between the slope at a particular point on the bandstructure and the Bloch mode

$$\frac{\partial \omega_n^2}{\partial k_x} = -\frac{1}{V} \int_{\text{cell}} \left[u_x^* \left(k_z u_z - i\frac{\partial u_z}{\partial z} + k_y u_y - i\frac{\partial u_y}{\partial y} \right) \right.$$
$$+ u_y^* \left(2i\frac{\partial u_y}{\partial x} - 2k_x u_y + k_y u_x - i\frac{\partial u_x}{\partial y} \right)$$
$$\left. + u_z^* \left(2i\frac{\partial u_z}{\partial x} - 2k_x u_z - i\frac{\partial u_x}{\partial z} + k_z u_x \right) \right] dV. \tag{32}$$

$\partial \omega_n^2 / \partial k_y$ and $\partial \omega_n^2 / \partial k_z$ are cyclic permutations of (32).

The second order of the expansion, $O(\mu^2)$, contains information about the curvature of the band, since the second-order correction to the eigenvalue can be written as

$$\lambda^{(2)} = \frac{1}{2} \left(\kappa_x^2 \frac{\partial^2 \omega_n^2}{\partial k_x^2} + \kappa_y^2 \frac{\partial^2 \omega_n^2}{\partial k_y^2 + \kappa_z^2 \frac{\partial^2 \omega_n^2}{\partial k_z^2}} + \kappa_x \kappa_y \frac{\partial^2 \omega_n^2}{\partial k_x \partial k_y} \right.$$
$$\left. + \kappa_y \kappa_z \frac{\partial^2 \omega_n^2}{\partial k_y \partial k_z} + \kappa_x \kappa_z \frac{\partial^2 \omega_n^2}{\partial k_x \partial k_z} \right). \tag{33}$$

If we project the all of the second-order terms in (26) to $1/V \langle \mathbf{u}_{n\mathbf{k}}|$, we obtain

$$\lambda^{(2)} = \frac{1}{V} \left[\kappa_x^2 (\langle \mathbf{u}_{n\mathbf{k}}|\mathbf{u}_{n\mathbf{k}}\rangle - \langle \mathbf{u}_{n\mathbf{k}}^{\mathbf{x}}|\mathbf{u}_{n\mathbf{k}}^{\mathbf{x}}\rangle) \right.$$
$$+ \kappa_y^2 (\langle \mathbf{u}_{n\mathbf{k}}|\mathbf{u}_{n\mathbf{k}}\rangle \langle \mathbf{u}_{n\mathbf{k}}^{\mathbf{y}}|\mathbf{u}_{n\mathbf{k}}^{\mathbf{y}}\rangle) + \kappa_z^2 (\langle \mathbf{u}_{n\mathbf{k}}|\mathbf{u}_{n\mathbf{k}}\rangle$$
$$- \langle \mathbf{u}_{n\mathbf{k}}^{\mathbf{z}}|\mathbf{u}_{n\mathbf{k}}^{\mathbf{z}}\rangle) + \kappa_x \kappa_y (\langle \mathbf{u}_{n\mathbf{k}}^{\mathbf{y}}|\mathbf{u}_{n\mathbf{k}}^{\mathbf{x}}\rangle + c.c.)$$
$$+ \kappa_y \kappa_z (\langle \mathbf{u}_{n\mathbf{k}}^{\mathbf{z}}|\mathbf{u}_{n\mathbf{k}}^{\mathbf{y}}\rangle + c.c.) + \kappa_x \kappa_z (\langle \mathbf{u}_{n\mathbf{k}}^{\mathbf{x}}|\mathbf{u}_{n\mathbf{k}}^{\mathbf{z}}\rangle + c.c.)$$
$$\left. - \sum_{m \neq n} \frac{|\langle \mathbf{u}_{m\mathbf{k}}|\mathbf{W}|\mathbf{u}_{n\mathbf{k}}\rangle|^2}{\omega_m^2 - \omega_n^2} \right] \tag{34}$$

where $|\mathbf{u}_{n\mathbf{k}}^{\mathbf{x}}\rangle$, $|\mathbf{u}_{n\mathbf{k}}^{\mathbf{y}}\rangle$, and $|\mathbf{u}_{n\mathbf{k}}^{\mathbf{z}}\rangle$ are the three vectorial components of the Bloch mode. In arriving at (34), we made an important assumption that $|\mathbf{u}_{m\mathbf{k}}\rangle$ is orthogonal to $|\mathbf{u}_{n\mathbf{k}}\rangle$. This approximation holds true for the lower bands and is verified numerically. The inner product between a Bloch mode from the first few bands and modes of higher bands is about 19 orders of magnitude smaller than its own magnitude.

Following a similar procedure to that used in the $O(\mu)$ analysis, we can separate the terms based on the perturbation parameters to arrive at expressions for the band curvatures

$$\frac{\partial^2 \omega_n^2}{\partial k_x^2} = \frac{2}{V} \left[(\langle \mathbf{u}_{n\mathbf{k}}|\mathbf{u}_{n\mathbf{k}}\rangle - \langle \mathbf{u}_{n\mathbf{k}}^{\mathbf{x}}|\mathbf{u}_{n\mathbf{k}}^{\mathbf{x}}\rangle) \right.$$
$$\left. - \sum_{m \neq n} \frac{|\langle \mathbf{u}_{m\mathbf{k}}|\widetilde{\mathbf{W}}_x|\mathbf{u}_{n\mathbf{k}}\rangle|^2}{\omega_m^2 - \omega_n^2} \right] \tag{35}$$

$$\frac{\partial^2 \omega_n^2}{\partial k_x k_y} = \frac{2}{V} \left[(\langle \mathbf{u}_{n\mathbf{k}}^{\mathbf{y}}|\mathbf{u}_{n\mathbf{k}}^{\mathbf{x}}\rangle + c.c.) \right.$$
$$\left. - 2 \sum_{m \neq n} \frac{Re\left[\langle \mathbf{u}_{m\mathbf{k}}|\widetilde{\mathbf{W}}_x|\mathbf{u}_{n\mathbf{k}}\rangle \langle \mathbf{u}_{m\mathbf{k}}|\widetilde{\mathbf{W}}_y|\mathbf{u}_{n\mathbf{k}}\rangle \right]}{\omega_m^2 - \omega_n^2} \right] \tag{36}$$

and $\partial^2 \omega_n^2 / \partial k_y^2$, $\partial^2 \omega_n^2 / \partial k_z^2$, $\partial^2 \omega_n^2 / \partial k_y k_z$, and $\partial^2 \omega_n^2 / \partial k_x k_z$ are cyclic permutations of (35) and (36). We have used our lower band approximation as in (34) in arriving at the curvature relations. Our analysis is now complete; we can relate band curvatures to the corresponding Bloch modes.

ACKNOWLEDGMENT

REFERENCES

[1] J. D. Joannopoulos, R. D. Meade, and J. N. Winn, *Photonic Crystals: Molding the Flow of Light*. Princeton, NJ: Princeton Univ. Press, 1995.
[2] S. Y. Li, E. Chow, V. Hietala, P. R. Villeneuve, and J. D. Joannopoulos, "Experimental demonstration of guiding and bending of electromagnetic waves in a photonic crystal," *Science*, vol. 282, no. 5387, pp. 274–276, Oct. 1998.
[3] M. Loncar, T. Doll, J. Vuckovic, and A. Scherer, "Design and fabrication of silicon photonic crystal optical waveguides," *IEEE J. Lightwave Technol.*, vol. 18, pp. 1402–1411, Oct. 2000.

 [4] S. G. Johnson, P. R. Villeneuve, S. Fan, and J. D. Joannopoulos, "Linear waveguides in photonic-crystal slabs," *Phys. Rev. B*, vol. 62, no. 12, pp. 8212–8222, Sept. 2000.
 [5] A. Adibi, Y. Xu, R. K. Lee, A. Yariv, and A. Scherer, "Properties of the slab modes in photonic crystal optical waveguides," *IEEE J. Lightwave Technol.*, vol. 18, pp. 1554–1564, Nov. 2000.
 [6] C. Weisbuch, H. Benistry, S. Olivier, M. Rattier, C. J. M. Smith, and T. F. Krauss, "3D control of light in waveguide-based two-dimensional photonic crystals," *IEICE Trans. Commun.*, vol. E84-B, no. 5, pp. 1286–1294, May 2001.
 [7] J. P. Albert, C. Jouanin, D. Cassagne, and D. Bertho, "Generalized Wannier function method for photonic crystals," *Phys. Rev. B*, vol. 61, no. 7, pp. 4318–4384, Feb. 2000.
 [8] J. P. Albert, C. Jouanin, D. Cassange, and D. Bertho, "Photonic crystal modeling using a tight-binding wannier function method," *Opt. Quantum Elect.*, vol. 32, pp. 251–263, Jan. 2002.
 [9] A. Yariv, "A coupled wave formalism for optical waveguiding by transverse Bragg reflection," *Opt. Lett.*, vol. 27, no. 11, pp. 936–938, June 2002.
[10] M. Charbonneau-Lefort, E. Istrate, M. Allard, J. Poon, and E. H. Sargent, "Photonic crystal heterostructures: Waveguiding phenomena and methods of solution in an envelope function picture," *Phys. Rev. B*, vol. 65, no. 125318, Mar. 2002.
[11] J. Kevorkian, *Partial Differential Equations: Analytical Solutions and Techniques*.   New York: Springer, 2000.
[12] C. M. de Sterke and J. E. Sipe, "Envelope-function approach for the electrodynamics of nonlinear periodic structures," *Phys. Rev. A*, vol. 38, no. 10, pp. 5149–5165, Nov. 1988.
[13] Q. Zhu and H. Kroemer, "Interface connection rules for effective-mass wave functions at an abrupt heterojunction between two different semiconductors," *Phys. Rev. B*, vol. 27, no. 6, pp. 3519–3527, Mar. 1983.
[14] I. Galbraith and G. Duggan, "Envelope-function matching conditions for GaAs/(Al,Ga)As heterojunctions," *Phys. Rev. B*, vol. 38, no. 14, pp. 10 057–10 059, Nov. 1988.
[15] A. A. Grinberg and S. Luryi, "Electron transmission across an interface of different one-dimensional crystals," *Phys. Rev. B*, vol. 39, no. 11, pp. 7466–7475, Apr. 1989.
[16] B. A. Foreman, "Connection rules versus differential equations for envelope functions in abrupt heterostructures," *Phys. Rev. Lett.*, vol. 80, no. 17, pp. 3823–3826, Apr. 1998.
[17] A. Chutinan and S. Noda, "Design for waveguides in three-dimensional photonic crystals," *Jpn. J. Appl. Phys.*, vol. 39, no. 1 4B, pp. 2533–2356, Apr. 2000.
[18] A. Adibi, Y. Xu, R. K. Lee, A. Yariv, and A. Scherer, "Guiding mechanisms in dielectric-core photonic-crystal optical waveguides," *Phys. Rev. B*, vol. 64, no. 3, July 2001.
[19] S. G. Johnson and J. D. Joannopoulos, "Block-iterative frequency-domain methods for maxwell's equations in a planewave basis," *Opt. Exp.*, vol. 8, no. 3, pp. 173–190, Jan. 2001.
[20] T. A. Birks, J. C. Knight, B. J. Mangan, and P. St. J. Russel, "Photonic crystal fibers: An endless variety," *IEICE Trans. Commun.*, vol. E84-B, no. 5, pp. 1211–1218, May 2001.
[21] S. Olivier *et al.*, "Mini-stopbands of a one-dimensional system: The channel waveguide in a two-dimensional photonic crystal," *Phys. Rev. B*, vol. 63, no. 113311, Mar. 2001.
[22] N. A. R. Bhat and J. E. Sipe, "Optical pulse propagation in nonlinear photonic crystals," *Phys. Rev. E*, vol. 64, no. 056604, Oct. 2001.
[23] J. E. Sipe, "Vector $k \cdot p$ approach for photonic band structures," *Phys. Rev. E*, vol. 62, no. 4, pp. 5672–5677, Oct. 2000.

Joyce Poon (S'02) received the B.A.Sc. degree in engineering science (physics option) from the University of Toronto, Toronto, ON, Canada in 2002. She is currently working toward the Ph.D. degree in electrical engineering at the California Institute of Technology, Pasadena, CA.

Her research interests include periodic photonic structures and optical resonators.

Emanuel Istrate (S'96) received the B.A.Sc. degree in engineering science from the University of Toronto, Toronto, ON, Canada, where he is currently working toward the Ph.D. degree in the Department of Electrical and Computer Engineering.

His research interests include photonic crystals and modeling of photonic structures.

Mathieu Allard (S'99) received the B.S. and M.S. degrees in engineering physics from Ecole Polytechnique de Montreal, Montreal, QC, Canada, in 1996 and 1998. He is currently working toward the Ph.D. degree in electrical engineering at University of Toronto, Toronto, ON, Canada, in the field of colloidal photonic crystals.

His research interests comprise photonic crystals and other novel photonic materials and the application of advanced numerical methods to the analysis of photonic structures.

Edward H. Sargent (S'97–M'98) holds the Nortel Networks—Canada Research Chair in Emerging Technologies at the University of Toronto, Toronto, ON, Canada. His contributions have led to well over 100 contributed and invited papers in refereed journals, conference proceedings, and institutional lectures in IEEE, the Optical Society of America, American Institute of Physics, and Materials Research Society publications and conferences. In 2001, the Canada Research Chairs Foundation wrote that he has "...shown that a new kind of photonic macrocrystal—one which harnesses nature's underlying drive toward symmetry—will transform how communication networks are built."

Dr. Sargent has chaired conferences and symposia, including the Photonic Networks Symposium at IEEE Globecom and the first Canada-France Conference on Molecular Photonics and Plastic Electronics. He received the 2002 IEEE Canada Outstanding Engineer Award for "for groundbreaking research in applying new phenomena and materials from nanotechnology towards transforming fibre-optic communications systems into agile optical networks." In 2002, the Canadian Institute for Advanced Research named him one of the nation's top 20 researchers under age 40 across the natural sciences, engineering, and social sciences.